Sustainable Water Resources Management (2026) 12:14
https://doi.org/10.1007/s40899-026-01324-w

ORIGINAL ARTICLE

Examining alternative crop suggestions under drought conditions induced by the climate change

Umut Suzan[1] · Mehmet Ali Ul[1] · Umut Okkan[2]

Received: 23 May 2025 / Accepted: 8 January 2026 / Published online: 9 February 2026

Abstract

Climate change impacts are becoming increasingly pronounced in Türkiye, with projections indicating further intensification in the coming decades. This study assesses potential hydro-meteorological changes in the Sarıgöl Afşar Dam Basin under RCP4.5 and RCP8.5 scenarios and proposes adaptive cropping strategies to mitigate drought impacts. Observed climate data (1986–2005) were statistically downscaled using NCEP/NCAR reanalysis and ensemble climate models to project temperature and precipitation for 2021–2050. Streamflow was simulated with the Dynamic Water Budget Model (DWBM), which incorporated twelve commonly used potential evapotranspiration (EPOT) equations—temperature-based, radiation-based, and combination approaches—within a precipitation–runoff framework. Model performance was evaluated using RMSE, R^2, NSE, RSR, and PBIAS, identifying the Hamon method as the most reliable. Crop evapotranspiration (ET_c) and irrigation water requirements (IWR) were estimated for grapevines (the dominant crop) and potential alternatives based on FAO-56 crop coefficients. Results show that continued grape monoculture would increase net IWR by 18.21% under RCP4.5 and 25.93% under RCP8.5 relative to the baseline (1986–2005). In contrast, the proposed mixed-cropping scenario—40% grape and 60% olive cultivation—would limit these increases to 11.9% and 15.6%, respectively. Secondary scenarios involving winter wheat and sunflower, evaluated as a comparative reference to illustrate the lower water-demand characteristics of annual crops, also exhibited comparatively lower water demands. Integrating EPOT-based hydrological modeling with climate projections provides a robust framework for irrigation planning and supports the design of resilient, water-efficient cropping systems under future climate conditions.

Keywords Climate crisis · Alternative cropping · Irrigation water requirement · Drought adaptation

Introduction

Natural climate variations—particularly droughts and floods—have long shaped Türkiye's environmental and socioeconomic systems, and their frequency and intensity are projected to increase in the coming decades. As extreme climate events intensify, they generate region-specific adverse impacts on ecosystems, water resources, and human livelihoods. Consequently, examining the spatial and temporal characteristics, predictability, and direct consequences of climate change has become essential. In this regard, assessing the regional manifestations of global climate change represents a major scientific priority (Demirgul et al. 2022; Wang et al. 2019).

Multiple studies have underscored Türkiye's high vulnerability to climate change, with its impacts expected to escalate in the near future (Fide 2022; Demirgul et al. 2022). Building on this evidence, the present research focuses on the Sarıgöl Afşar Dam Basin in western Türkiye—a region characterized by high agricultural potential and recognized for the cultivation of the renowned Sultaniye Seedless grape variety (MAF 2023). Recent observations indicate a substantial decline in the Afşar Dam water level, now falling below the critical sustainability threshold (Bayram 2022).

Identifying alternative cropping patterns has therefore become crucial for mitigating the adverse effects of climate change on agricultural productivity. The selection of crops with lower water requirements and higher tolerance

✉ Umut Suzan
umut.suzan@ege.edu.tr

[1] Department of Agricultural Structures and Irrigation, Faculty of Agriculture, Ege University, Izmir, Turkey

[2] Department of Civil Engineering, Faculty of Engineering, Balıkesir University, Balıkesir, Turkey

to abiotic stresses—such as elevated temperature and salinity—offers a strategic pathway to maintaining food security and rural livelihoods under increasing water scarcity (Lee et al. 2022). Beyond short-term adaptation, diversified cropping systems also strengthen the long-term resilience of agricultural production to future climatic extremes.

This study extends climate projections to the year 2050, using hydrological observations from 1986 to 2005 as the reference baseline. Combined climate model approaches were employed to assess the hydrological implications of projected temperature and precipitation changes. Streamflow simulations were performed with the Dynamic Water Budget Model (DWBM), which has recently gained prominence for its robust representation of hydrological processes under climate variability (Ahn and Merwade 2014). By integrating twelve empirical formulations of potential evapotranspiration (EPOT) with observed streamflow data, the DWBM provides a reliable framework for water-balance-based simulations. EPOT serves as a critical component in hydrological modeling, particularly for estimating crop water use and irrigation requirements under climate change conditions (Allen et al. 1998; McMahon et al. 2013).

Accordingly, this study evaluates alternative cropping strategies, estimates crop water consumption, and quantifies irrigation water requirements based on observed and projected meteorological data. The overall aim is to maintain current agricultural productivity while supporting proactive adaptation measures for sustainable water management under future climate risks.

Materials and methods

Study area and climate data collection

The study area is situated in Manisa Province, where the continental climate of Central Anatolia interacts with the Mediterranean climate. While the influence of the continental climate is more pronounced in the surrounding highlands and plateaus, the Mediterranean climate predominates across the plains and valleys (MAF 2023). The Sarıgöl Afşar Dam Basin—renowned for producing the world-famous "Sultaniye Seedless" grape—represents an agriculturally important region that typifies the climatic characteristics of Manisa. The Afşar Dam, with a structural volume of 3.17×10^6 m^3, a normal reservoir capacity of 69 hm^3, a height of 46 m from the riverbed, and a lake surface area of 5.25 km^2, provides a vital water supply that sustains agricultural production within the basin (SHW 2021). Land use and land cover (LULC) characteristics of the study area are illustrated in Fig. 1.

Because the basin's drainage area is relatively small (< 500 km^2; 119 km^2), climate variables were analyzed on an areal basis. Long-term mean annual values of average temperature (T_{ave}), maximum temperature (T_{max}), minimum temperature (T_{min}), and precipitation (P) were obtained from the Sarıgöl and Alaşehir meteorological stations, which are representative of the basin, and are summarized in Table 1. Streamflow data were derived from the TÜBİTAK-supported research project No. 114Y716 (Okkan et al. 2016), and the corresponding mean values are also presented in Table 1.

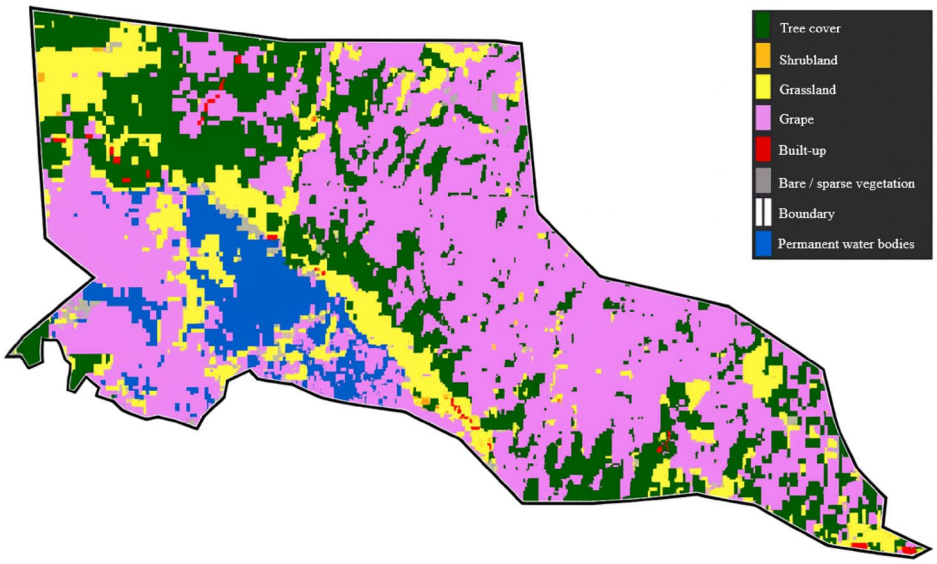

Fig. 1 Sarigol afsar dam land use/land cover map (FAO 2025)

Table 1 Long-term mean annual hydro-meteorological variables observed at the stations

Average Temperature (°C)	Maximum Temperature (°C)	Minimum Temperature (°C)	Precipitation (mm yr^{-1})	Flow (mm)
16.9	36.5	4.3	418.46	7.6

Flow values represent long-term monthly averages expressed in depth units (mm) for consistency with precipitation data

Dynamic water budget model (DWBM)

The DWBM was developed to simulate streamflow and assess irrigation water requirements. Detailed descriptions of the model structure and methodology can be found in earlier studies (Okkan 2015; Kiymaz 2018; Okkan and Kiymaz 2020). In this study, P, observed streamflow, and EPOT served as input variables, while the modeled streamflow (Q_m) was obtained as the primary model output. Within the DWBM framework, the model operates on a monthly water balance, where $Q_{m(t)}$ is expressed as the sum of direct runoff, $Q_{d(t)}$, and baseflow, $Q_{b(t)}$:

$$Q_{m(t)} = Q_{d(t)} + Q_{b(t)} \quad (1)$$

In this configuration, precipitation, potential evapotranspiration, and observed streamflow constitute the key inputs that indirectly determine surface runoff and baseflow components. This parsimonious parameterization allows the model to reproduce monthly streamflow dynamics even under limited data conditions (Perrin et al. 2001; Okkan 2015).

In the DWBM structure, soil moisture dynamics are implicitly represented through monthly water balance components, with variations in soil storage modeled as a function of precipitation, evapotranspiration, and groundwater recharge. Although land use and cropping patterns are not explicitly defined as input parameters, their effects are indirectly reflected through EPOT and observed streamflow data, representing basin-scale hydrological responses. This conceptual framework thus enables effective flow simulation under data-scarce conditions, consistent with previous DWBM applications (Fenicia et al. 2011; Okkan 2015).

Accordingly, this study focused on the most frequently cited and widely applied EPOT equations in the literature. These equations were grouped into two main categories: (i) temperature-based equations, including Thornthwaite (Thw), Blaney–Criddle (Bl–Cr), and Hamon (Ham); and (ii) radiation-based equations, which require more detailed meteorological datasets, such as Turc, Makkink (Mak), Hargreaves (Harg), Priestley–Taylor (Prs–Tyl), Jensen–Haise (J–H), Caprio (Cpr), Irmak (Irm), and McGuinness–Bordne (McG–Bor). Additionally, the Penman–Monteith (Pen–Mon) equation—requiring the most comprehensive set of climatic inputs—was applied as a representative combination approach (Kiymaz 2018; Oudin et al. 2005a, b).

The complete formulations, parameter definitions, and bibliographic references for all twelve EPOT equations (Allen et al. 1998; Blaney and Criddle 1950; Caprio 1974; Hargreaves and Samani 1985; Heydari et al. 2014; Irmak et al. 2003; Jensen and Haise 1963; Makkink 1957; McGuinness and Bordne 1972; Monteith 1965; Pandey et al. 2016; Penman 1948; Priestley and Taylor 1972; Thornthwaite 1948; Turc 1961; Xu and Singh 2000, 2001, 2002; Xystrakis and Matzarakis 2011) are provided in the Supplementary Material. Model performance for each EPOT-based simulation was then evaluated using the statistical criteria described in Sect. "Model Evaluation Criteria".

Among the twelve EPOT formulations tested, the Hamon method—identified as the best-performing approach for this basin—is presented below as a representative example. The Hamon equation (Hamon 1961) estimates potential evapotranspiration as:

$$EPOT = 0.55x29.8xD^2xe^{(0.062xT_{ave})} \quad (2)$$

where D is the mean day length (hours).

Model evaluation criteria

The performance of the DWBM and the alternative EPOT-based models was assessed using several widely accepted statistical indicators, including the root mean square error (RMSE), coefficient of determination (R2), Nash–Sutcliffe efficiency (NSE), the ratio of RMSE to the standard deviation of observed data (RSR), and percent bias (PBIAS), following the standard formulations outlined by Moriasi et al. (2007).

RMSE quantifies the overall magnitude of deviation between simulated and observed values, whereas R2 represents the proportion of variance in the observed data that is explained by the model. NSE evaluates the model's predictive capability by comparing its performance to that of the mean of the observed data. RSR expresses RMSE as a ratio to the standard deviation of the observed dataset, providing a normalized measure of error magnitude. PBIAS quantifies the model's systematic tendency to overestimate or underestimate observations.

Together, these complementary criteria offer a comprehensive statistical basis for evaluating model accuracy and identifying the most reliable EPOT formulation for subsequent analysis.

Table 2 Crop coefficient (Kc) values of currently and potentially cultivated crops in the study area

Agricultural Products	January	February	March	April	May	June	July	August	September	October	November	December
Olive and Olive Oil	–	–	0.57	0.57	0.57	0.87	0.87	0.87	0.87	0.87	0.47	0.47
2nd Product Sunflower	–	–	–	–	–	–	0.37	0.73	0.77	0.77	–	–
Tomato Paste	–	–	–	–	–	–	0.05	1.09	0.37	0.37		
Beans	0.8	1.16	1.16	1.16	0.27	0.27	–	–	–	–	0.8	0.8
Grape	–	–	0.24	0.24	0.24	1.17	1.17	0.83	0.83	0.83	–	–
Melon	–	–	0.38	0.38	1.07	0.93	–	–	–	–	–	–
Eggplant	–	–	–	–	0.15	0.15	1.07	0.76	0.76	–	–	–
Cabbage	–	–	–	0.19	0.19	1.08	1.08	0.92	0.92	–	–	–
Winter Wheat	0.34	1.05	1.05	1.05	0.95	0.95	–	–	–	–	0.34	0.34
Watermelon	–	–	0.52	0.52	1.01	0.77	–	–	–	–	–	–
arley	0.8	1.16	1.16	0.26	0.26	–	–	–	–	–	0.8	0.8
Potatoes	–	–	0.54	1.16	1.16	0.77	–	–	–	–	–	–

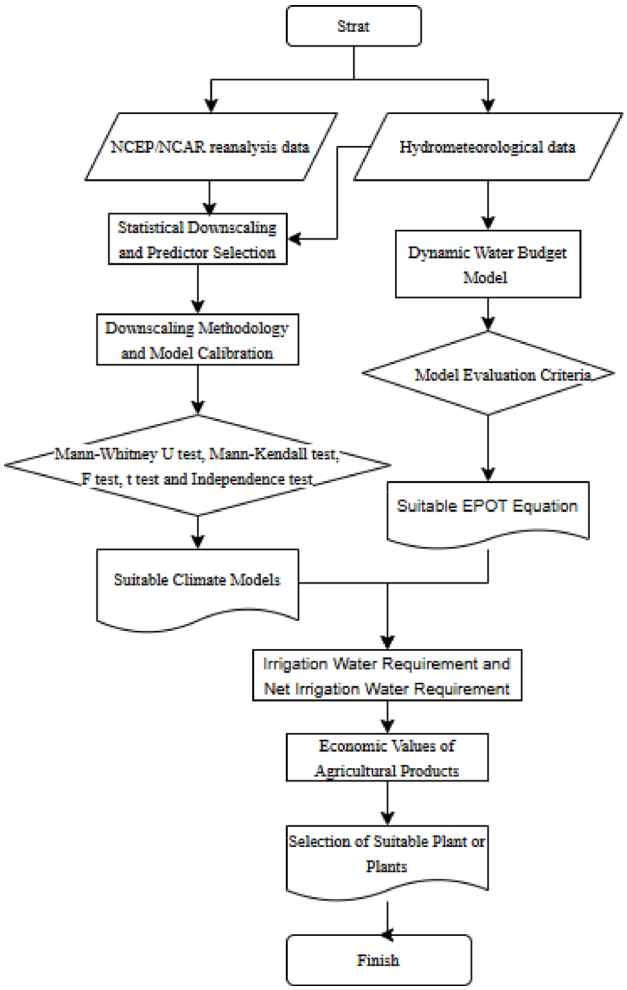

Fig. 2 Flow chart of the study

Statistical downscaling and predictor selection

In addition to meteorological station observations, NCEP/NCAR reanalysis data for the period 1986–2005 were utilized as the basis for constructing statistical downscaling models (Raziei and Parehkar 2021). Standard approaches for predictor selection were employed, including linear regression and correlation-based screening methods. For example, Okkan and Inan (2015) examined the relationships between observed climate variables and NCEP/NCAR reanalysis predictors using a correlation matrix and identified potential predictors with correlation coefficients exceeding 0.30. Based on these selected predictors, statistical downscaling models were subsequently developed to estimate temperature and precipitation at the basin scale (Liu et al. 2023).

Downscaling methodology and model calibration

The optimal combination of NCEP/NCAR reanalysis variables for the statistical downscaling models was determined

using the All Possible Regressions (APREG) method. APREG systematically evaluated all potential predictor combinations and identified the most suitable set based on statistical performance metrics, including the coefficient of determination (R^2), root mean square error (RMSE), and the difference in RMSE (ΔRMSE) (Hocking 1976; Burnham and Anderson 2002). The selected predictors were then employed as inputs for downscaling models developed through the integration of Hybrid Particle Swarm Optimization (HPSO) with Artificial Neural Networks (ANN) (Maraun et al. 2010; Okkan and Inan 2015).

The model was developed using hydrometeorological data from 1986 to 2005. The first ten years (1986–1995) were used for calibration (training), while the subsequent ten years (1996–2005) were reserved for validation (testing). The downscaling framework was further extended to include future climate projections under the RCP4.5 and RCP8.5 emission scenarios, consistent with the climate projections presented in the IPCC Fifth Assessment Report (AR5). A suite of general circulation models (GCMs) representing both historical and future climate conditions was analyzed, including BCC-CSM1.1, CCSM4, CESM1 (CAM5), CSIRO-Mk3.6.0, GFDL-CM3, GFDL-ESM2M, HadGEM2-ES, IPSL-CM5A-LR, MIROC-ESM, and MRI-CGCM3.

Evaluation of climate models and streamflow estimation

Based on basin-scale temperature and precipitation data, the climate models employed in this study were statistically evaluated, revealing variations in both their distributions and statistical characteristics. Several nonparametric and parametric statistical tests—including the Mann–Whitney U test (Wilcoxon 1945), Mann–Kendall trend test (Mann 1945; Kendall 1975), F-test (Fisher 1925), t-test (Student 1908), and independence test (Wald and Wolfowitz 1940)—were applied to compare model-based scenario outputs representing current climate conditions with the observed dataset.

The evaluation indicated that ensemble climate models, constructed by combining appropriately selected individual models, produced more reliable projections for future periods. Accordingly, temperature and precipitation changes for the 2021–2050 period were estimated under the RCP4.5 and RCP8.5 scenarios. The DWBM was subsequently applied to estimate future streamflow by integrating potential evapotranspiration (EPOT) values derived from the Hamon empirical equation with precipitation inputs obtained from the RCP scenarios (Abdulla and Lettenmaier 1997).

The resulting streamflow projections revealed potential future trends in flow volumes under changing climate conditions, indicating a likely decrease in water availability for irrigation purposes. All statistical tests were applied following their standard formulations and in accordance with widely accepted hydrological applications in the literature (Okkan 2013; Helsel and Hirsch 2002).

Irrigation water requirement calculation

Lastly, to estimate crop water consumption, EPOT values were multiplied by the crop coefficients (K_c) of grapevines—the dominant crop in the basin—as well as those of other potential crops (FAO56 1998). The corresponding crop coefficients are presented in Table 2 (GDARP and SHW 2016). Because the length and timing of the growing season vary among crops, comparisons were made based on irrigation water requirement (IWR) values corresponding to each crop's specific growing period.

The IWR for the basin was calculated by subtracting effective precipitation from the estimated crop water consumption. Subsequently, the IWR was multiplied by the currently irrigated area (11,830 ha) to determine the net irrigation water requirement (net IWR) (Serbes et al. 2018). In this study, "net IWR" refers to the volume of water that

Table 3 Performance of the DWBM based on the EPOT equations during the calibration and validation periods

Calibration Period					Verification Period			
Method Name	RMSE (mm)	R^2	NS	PBIAS (%)	RMSE (mm)	R^2	NS	PBIAS (%)
Cpr	5.89	0.57	0.56	-6.81	5.89	0.57	0.56	-6.81
Ham	4.88	0.70	0.70	4.93	4.88	0.70	0.70	4.93
Harg	6.11	0.54	0.53	-9.52	6.11	0.54	0.53	-9.52
Irm	5.96	0.56	0.55	-6.71	5.96	0.56	0.55	-6.71
J-H	6.00	0.56	0.55	-8.32	6.00	0.56	0.55	-8.32
Mak	6.07	0.55	0.54	-8.86	6.07	0.55	0.54	-8.86
McG-Bor	5.73	0.59	0.59	-2.34	5.73	0.59	0.59	-2.34
Pen-Mon	6.08	0.55	0.54	-9.17	6.08	0.55	0.54	-9.17
Prs-Tyl	5.79	0.58	0.58	-3.37	5.79	0.58	0.58	-3.37
Thw	4.75	0.72	0.72	3.08	4.75	0.72	0.72	3.08
Turc	6.05	0.55	0.54	-9.23	6.05	0.55	0.54	-9.23
Bl-Cr	5.86	0.57	0.57	-3.41	5.86	0.57	0.57	-3.41

Table 4 Correlation coefficients between NCEP/NCAR reanalysis data and observed meteorological data

	SLP	Rhum	Press	Prate	Air	hgt200	air200	rhum500	hgt500	air500	rhum850	hgt850	air850
T_{ave}	-0.82	-0.93	-0.74	-0.58	0.99	0.95	0.70	-0.85	0.93	0.96	-0.71	0.41	0.99
T_{max}	-0.78	-0.90	-0.71	-0.57	0.96	0.92	0.64	-0.82	0.91	0.93	-0.73	0.41	0.96
T_{min}	-0.83	-0.91	-0.76	-0.54	0.97	0.93	0.73	-0.84	0.90	0.94	-0.66	0.36	0.96
P	**0.28**	0.67	**0.21**	0.75	-0.60	-0.61	-0.41	0.66	-0.64	-0.59	0.66	-0.55	-0.60

Air, air200, air500, air850: Air temperature at surface, 200, 500, and 850 hPa (K; converted to °C for analysis); hgt200, hgt500, hgt850: geopotential height at 200, 500, and 850 hPa (m); Rhum, rhum500, rhum850: Relative humidity at surface, 500, and 850 hPa (%); Prate: Precipitation rate (mm/s); SLP, Press: Sea level pressure and surface pressure (hPa)

must be supplied to the crop root zone, excluding conveyance and application losses. Although these losses were not incorporated into the present calculations, they are typically assumed to range between 15 and 25% for application and 5–10% for conveyance in the literature (FAO56 1998; GDARP and SHW 2016).

The effective root zone depth for grapevines was assumed to be approximately 1.0 m, in accordance with FAO guidelines. The overall methodological framework applied in this study is summarized in the flowchart presented in Fig. 2.

Results and discussion

Model performance evaluation

The performance of the DWBM, developed using alternative EPOT formulations, was evaluated for both the calibration and validation periods using standard performance metrics—RMSE (mm), R2, NSE, and PBIAS (%). These assessments were conducted based on observed streamflow data along with precipitation and potential evapotranspiration inputs. The results demonstrated that the Hamon method yielded the most consistent and reliable performance. During the calibration period, RMSE, R2, NSE, and PBIAS values were 4.88 mm, 0.70, 0.70, and 4.93%, respectively, whereas in the validation period, the corresponding values were 8.27 mm, 0.69, 0.68, and 7.66%. Although the FAO Penman–Monteith method is theoretically considered the most physically representative—accounting for both energy balance and aerodynamic components—the comparative evaluation for the Afşar Basin indicated that the Hamon method provided more accurate predictions. This finding underscores the significance of local basin characteristics and data limitations, whereby the Hamon approach outperformed other EPOT formulations in terms of statistical performance (Table 3).

EPOT estimation, one of the most critical inputs for precipitation–runoff modeling, can be derived from temperature-based, radiation-based, mass-transfer, or combination approaches (Oudin et al. 2005a, b). A rigorous evaluation is therefore required to identify the most suitable formulation for a given basin. While several studies have reported satisfactory performance of the Penman–Monteith (Pen–Mon) equation and its derivatives—primarily due to their consistency with lysimeter measurements (Kiymaz 2018)—other research indicates that Pen–Mon does not consistently yield optimal results. For instance, Oudin et al. (2005b) developed precipitation–runoff models using 27 different EPOT formulations and demonstrated that the McG–Bor equation produced more reliable hydrological simulations than alternative methods. Similarly, several studies have reported

Table 5 Selection of predictors for the T_{ave} estimation using areal data from the Alaşehir and Sarigol stations

Vars	R^2	RMSE	ΔRMSE	SLP	Rhum	Press	Prate	Air	hgt200	air200	rhum500	hgt500	air500	rhum850	hgt850	air850
1	97.7	1.21						X								
2	98.5	0.98	23.52					X	X							
3	98.7	0.92	6.91					X				X				X
4	98.8	0.87	4.66					X	X	X						X
5	98.9	0.85	2.96					X	X	X			X			X
6	98.9	0.84	1.18					X	X	X	X		X			X
7	98.9	0.84	0.25					X	X	X	X		X	X		X
8	98.9	0.83	0.46		X			X	X	X	X		X	X		X
9	98.9	0.83	0.28			X		X	X	X	X	X	X	X		X
10	98.9	0.83	0.40		X	X		X	X	X	X	X	X	X		X
11	98.9	0.83	-0.06		X	X	X	X	X	X	X	X	X	X		X
12	98.9	0.83	-0.07	X	X	X		X	X	X	X	X	X	X	X	X
13	98.9	0.83	-0.09	X	X	X	X	X	X	X	X	X	X	X	X	X

Table 6 Selection of predictors for the T_{max} estimation using areal data from the Alaşehir and Sarıgöl stations

Vars	R^2	RMSE	ΔRMSE	SLP	Rhum	Press	Prate	Air	hgt200	air200	rhum500	hgt500	air500	rhum850	hgt850	air850
1	96	1.57														X
2	96.9	1.40	12.25									X				X
3	97	1.36	3.04		X							X				X
4	97.1	1.34	1.20	X	X				X							X
5	97.2	1.32	1.86		X				X	X				X		X
6	97.3	1.31	0.76		X				X	X			X	X		X
7	97.3	1.30	0.55		X				X	X		X	X		X	X
8	97.4	1.30	0.55	X	X				X	X		X	X		X	X
9	97.4	1.29	0.18	X	X	X			X	X		X	X		X	X
10	97.4	1.29	0.12	X	X	X			X	X	X	X	X	X		X
11	97.4	1.29	0.02	X	X	X			X	X	X	X	X	X	X	X
12	97.4	1.29	0.07	X	X	X		X	X	X	X	X	X	X	X	X
13	97.4	1.29	-0.16	X	X	X	X	X	X	X	X	X	X	X	X	X

Table 7 Selection of predictors for the T_{min} estimation using areal data from the Alaşehir and Sarıgöl stations

Vars	R^2	RMSE	ΔRMSE	SLP	Rhum	Press	Prate	Air	hgt200	air200	rhum500	hgt500	air500	rhum850	hgt850	air850
1	96.8	1.30						X								
2	97.7	1.10	17.64					X				X				
3	97.8	1.08	2.45					X				X				X
4	97.8	1.07	0.52					X	X	X						X
5	97.9	1.05	1.56					X	X	X			X			X
6	98	1.04	0.96					X	X	X	X			X		X
7	98	1.04	0.34					X	X	X	X		X	X		X
8	98	1.04	0.10					X	X	X	X	X	X	X		X
9	98	1.04	0.36			X		X	X	X	X	X	X	X		X
10	98	1.04	-0.10		X	X		X	X	X	X	X	X	X		X
11	98	1.04	-0.11	X	X	X		X	X	X	X	X	X	X		X
12	98	1.04	-0.15	X	X	X	X	X	X	X	X	X	X	X		X
13	98	1.04	-0.16	X	X	X	X	X	X	X	X	X	X	X	X	X

strong performance of the Hamon method under specific climatic and data-scarce conditions (Tokar and Momcilo 2000; Zainal and Toshiharu 2017).

APREG model results

A correlation matrix was computed to examine the relationships between NCEP/NCAR reanalysis variables and meteorological station data across the study region. Predictors with correlation coefficients exceeding 0.30 were selected for subsequent analysis. Based on this screening, T_{ave}, T_{max}, T_{min}, and thirteen additional predictors were used to construct the APREG model, resulting in $2^{13}-1=8191$ possible model combinations. For the precipitation dataset, however, the SLP (sea level pressure, hPa) and Press (surface pressure, hPa) variables showed correlation values below this threshold. Consequently, $2^{11}-1=2047$ regression models were developed for the P dataset (Table 4).

Previous studies have similarly emphasized the importance of NCEP/NCAR variables as predictors. For example, Okkan and Inan (2015) identified air (surface air temperature), air200 and air850 (air temperature at 200 and 850 hPa, respectively), hgt850 (geopotential height at 850 hPa), and prate (precipitation rate) as effective predictors in the Büyük Menderes Basin, with correlation coefficients (R) of ± 0.30 or higher. Kuskova et al. (2021) reported generally lower R values for precipitation than for temperature in a Eurasian-scale study, although most stations exhibited statistically significant correlations exceeding 0.8. Similarly, Nacar et al. (2022) observed high R values for temperature but lower values for precipitation in the Eastern Black Sea region, where maximum R for precipitation was 0.39 and temperature correlations did not exceed 0.96. These results confirm that the findings of the present study are consistent with the broader literature.

The APREG model constructed using T_{ave} data indicated that including additional NCEP/NCAR predictors did not significantly alter RMSE or R^2 values, suggesting that the air variable alone provided stable and reliable results (Table 5). For T_{max}, incorporating supplementary predictors slightly increased R^2 and decreased RMSE, although overall significance levels remained similar; the first selected variable (Vars) for T_{max} was air850 (Table 6). For T_{min}, results were consistent with those obtained for T_{ave} and T_{max}—the air variable again yielded robust estimates, while adding extra predictors marginally improved R^2 and reduced RMSE (Table 7).

When the P dataset was analyzed using the APREG method, eleven predictors were evaluated based on R2, RMSE, and ΔRMSE. Among these, prate (precipitation rate) and hgt500 (geopotential height at 500 hPa) demonstrated the strongest compatibility with the P dataset and

Table 8 Selection of predictors for the P estimation using areal data from the Alaşehir and Sarıgöl stations

Vars	R^2	RMSE	ΔRMSE	Rhum	Prate	Air	hgt200	air200	rhum500	hgt500	air500	rhum850	hgt850	air850
1	61	18.28			X									
2	65.1	17.33	5.49		X					X				
3	66.1	17.10	1.35		X					X	X			
4	68.5	16.50	3.59		X		X	X		X				
5	69.1	16.39	0.68		X		X	X		X				X
6	69.2	16.37	0.11		X		X	X	X	X				X
7	69.2	16.40	-0.15		X		X	X	X	X	X			X
8	69.3	16.42	-0.13		X		X	X	X	X	X		X	X
9	69.3	16.44	-0.14		X		X	X	X	X	X	X	X	X
10	69.3	16.47	-0.16	X	X		X	X	X	X	X	X	X	X
11	69.3	16.50	-0.16	X	X	X	X	X	X	X	X	X	X	X

Table 9 Performance of scale reduction models in the test period for monthly climatic data

	R^2	RMSE	NS	PBIAS	RSR
T_{ave}	0.98	1.02	0.98	0.00	0.13
T_{min}	0.97	1.38	0.96	0.02	0.18
T_{max}	0.96	1.52	0.96	0.00	0.19
P	0.70	15.62	0.70	1.81	0.55

were statistically significant at the 95% confidence level according to the ΔRMSE criterion. However, the inclusion of additional parameters did not lead to notable improvements (Table 8).

The applicability of the APREG approach has also been confirmed in other regions. For instance, Serbes et al. (2018) applied the method to the Menemen Basin using the 1961–1990 reference period. Their analysis yielded an RMSE of 0.836 and an R2 of 98.5% for temperature, with predictors including hgt850, air500 (air temperature at 500 hPa), hgt500, hgt200 (geopotential height at 200 hPa), and air. For precipitation, ten predictors were used, resulting in an R2 of 33.4% and an RMSE of 63.1%. These variations in predictor performance can be attributed to differences in the reference period and regional climatic characteristics. Other studies (Maraun et al. 2010; Panagos et al. 2022) have likewise employed the APREG method in various basins and timeframes, reporting comparable outcomes. Collectively, these findings indicate that while the overall performance of the APREG framework is robust, the type and number of effective predictors may vary depending on regional conditions and data structure.

Climate projections (2021–2050)

In this study, statistical downscaling models based on ANN integrating HPSO and the Levenberg–Marquardt algorithm were evaluated using the NSE, RSR, and PBIAS. The results indicated that the temperature and precipitation models exhibited similar behavior during the training phase. In the testing phase, the models achieved R2 values ranging from 0.70 to 0.98 and RMSE values between 15.62 and 1.02 for T_{ave}, T_{max}, T_{min}, and P. Accordingly, T_{ave}, T_{max}, and T_{min} were classified as "very good" based on NS, PBIAS, and RSR, whereas precipitation was rated as "good" (NS, RSR) and "very good" (PBIAS), with NS = 0.70, PBIAS = 1.81, and RSR = 0.55 (Table 9).

Within the framework of IPCC AR5, ten climate scenarios were applied through a multi-model ensemble approach to estimate the monthly distributions of T_{ave}, T_{max}, T_{min}, and P. The climate models yielding consistent results are listed in Tables 10, 11, 12 and 13. Similar multi-model projections developed for the Gomte Basin (24 models) and Tahtalı Basin (23 models) (Abeysingha et al. 2020; Okkan 2013) are in agreement with the findings of this study.

Table 10 Climate models that accurately simulate monthly precipitation

January	February	March	April	May	June	July	August	September	October	November	December
CCSM4-NCAR	CESM1(CAM5)	MIROC-ESM	MIROC-ESM	MIROC-ESM	BCC-CSM11	MIROC-ESM	Had-GEM-ES	GFDL-ESM2	HadGEM-ES	BCC-CSM11	MRI-CGCM3

Table 11 Climate models that accurately simulate monthly average temperatures

January	February	March	April	May	June	July	August	September	October	November	December
GFDL-CM3	BCC-CSM11	MIROC-ESM	CSIRO-Mk36	BCC-CSM11	Had-GEM-ES	GFDL-ESM2	MIROC-ESM	CESM1(CAM5)	HadGEM-ES	BCC-CSM11	MRI-CGCM3

Table 12 Climate models that accurately simulate monthly maximum temperatures

January	February	March	April	May	June	July	August	September	October	November	December
CSIRO-Mk36	CCSM4-NCAR	GFDL-CM3	CCSM4-NCAR	CSIRO-Mk36	CCSM4-NCAR	CESM1(CAM5)	Had-GEM-ES	IPSL-CM5A-LR	CSIRO-Mk36	MRI-CGCM3	CCSM4-NCAR

Table 13 Climate models that accurately simulate monthly minimum temperatures

January	February	March	April	May	June	July	August	September	October	November	December
IPSL-CM5A-LR	HadGEM-ES	BCC-CSM11	CCSM4-NCAR	CCSM4-NCAR	GFDL-CM3	GFDL-CM3	MIROC-ESM	GFDL-ESM2	GFDL-CM3	GFDL-CM3	CESM1(CAM5)

The ensemble projections consistently indicate an overall warming trend across all RCP scenarios, with annual temperature averages exceeding historical baselines. Monthly analyses show that the highest T_{ave} occurs in July, while the highest T_{max} is observed in November (Tables 14 and 15). The annual average T_{min} is projected to increase by 0.99 °C under RCP4.5 and 1.50 °C under RCP8.5 for the 2021–2050 period. The highest T_{min} is projected in November under RCP4.5, whereas RCP8.5 indicates increases extending from November through March (Table 16).

Precipitation projections exhibit a decreasing trend throughout the year, with the lowest values anticipated in July. Reductions are more pronounced under RCP8.5 compared to RCP4.5. Annual precipitation is projected to decrease by 9.33% under RCP4.5 and by 14.67% under RCP8.5 (Table 17).

According to the IPCC Sixth Assessment Report (AR6), global mean temperatures are expected to increase by approximately 2.5–4 °C by 2100 (Lee et al. 2022). Regional-scale studies also support this global warming tendency. For example, in Bangladesh, increases in T_{max} and T_{min} during 2021–2060 were most evident in February (Islam et al. 2021). In the Syr Darya Basin, T_{ave}, T_{max}, and T_{min} are projected to rise by 1.81–4.88 °C between 2021 and 2100 (Zhai et al. 2023). In China, annual temperature increases of 0.42–0.45 °C were reported for 2011–2040 under RCP8.5 (You et al. 2014). Despite regional variability, these findings collectively confirm the global consistency of increasing T_{ave}, T_{max}, and T_{min} trends.

Regarding precipitation, the Syr Darya Basin is projected to experience a 14.26–39.92% decline between 2021 and 2100 under RCP8.5 (Zhai et al. 2023). Similar downward trends have been documented across South and Central America (Chou et al. 2014), Denver (Jiang et al. 2016), and Europe (Panagos et al. 2022; Doulabian et al. 2021), aligning with the precipitation projections obtained in this study.

Flow projections (2021–2050)

The DWBM precipitation–runoff model utilized basin-specific hydro-meteorological time series as inputs to simulate streamflow. Using these datasets, simulations were performed for both the historical baseline period (1986–2005 water year) and the future RCP scenarios (2021–2050 water year). The results indicate that long-term monthly streamflow is projected to decline relative to historical conditions, with reductions estimated at approximately 15% under RCP4.5 and 28% under RCP8.5 (Fig. 3).

Comparable studies have reported similar trends of streamflow reduction under changing climate conditions. Özdemir (2021), for instance, examined the impacts of climate change on streamflow in the Yuvacık Dam Basin and projected decreases of 74%, 67%, and 55% for the Kazandere, Kirazdere, and Serindere sub-basins, respectively, under RCP4.5; corresponding reductions under RCP8.5 were 69%, 74%, and 64%. Likewise, Ayva et al. (2023), analyzing data from 1975 to 2000 for the Kirazdere Basin, concluded that increasing temperatures combined with declining precipitation would lead to decreased streamflow across both RCP scenarios. In another study, Singh and Singh (2022) projected reductions of approximately 64.4%

Table 14 Differences (Δt) in monthly average temperatures (°C) from the historical period based on the basin-scale downscaled combined climate model

Scenario	Period	January	February	March	April	May	June	July	August	September	October	November	December	Annual
RCP4.5	2021–2050	0.72	**1.30**	0.73	**1.31**	**1.02**	0.37	**1.54**	0.77	**1.26**	0.23	0.48	**0.69**	**0.87**
RCP8.5	2021–2050	**0.95**	**1.44**	**1.16**	**1.47**	**2.04**	0.46	**2.10**	**1.10**	**1.93**	0.38	**0.96**	**0.64**	**1.22**

*α = 0.05; bold parts indicate significant differences in the mean according to the t-test, gray shaded parts indicate non-homogeneous data according to the MW test

Table 15 Differences (Δt) in monthly maximum temperatures (°C) from the historical period based on the basin-scale downscaled combined climate model

Scenario	Period	January	February	March	April	May	June	July	August	September	October	November	December	Annual
RCP4.5	2021–2050	**1.99**	**1.45**	0.34	**1.40**	0.29	0.44	0.44	0.66	0.30	0.37	**2.71**	**1.63**	**1.00**
RCP8.5	2021–2050	**2.94**	**2.36**	0.51	**1.59**	**0.81**	**1.08**	**0.71**	**1.17**	**1.45**	0.49	**2.99**	**2.04**	**1.51**

*α = 0.05; bold parts indicate significant differences in the mean according to the t-test, gray shaded parts indicate non-homogeneous data according to the MW test

Table 16 Differences (Δt) in monthly minimum temperatures (°C) from the historical period based on the basin-scale downscaled combined climate model

Scenario	Period	January	February	March	April	May	June	July	August	September	October	November	December	Annual
RCP4.5	2021–2050	**1.49**	**1.86**	**2.11**	0.42	0.54	0.77	0.74	0.41	0.58	0.14	**2.20**	0.59	**0.99**
RCP8.5	2021–2050	**1.95**	**2.25**	**2.64**	**1.13**	**1.14**	**0.81**	**0.98**	**0.88**	**1.35**	**1.13**	**2.64**	**1.18**	**1.50**

*α = 0.05; bold parts indicate significant differences in the mean according to the t-test, gray shaded parts indicate non-homogeneous data according to the MW test

Table 17 Percentage differences in monthly precipitation (mm) from the historical period based on the basin-scale downscaled combined climate model

Scenario	Period	January	February	March	April	May	June	July	August	September	October	November	December	Annual
RCP4.5	2021–2050	-9.40	-3.86	-9.18	-10.95	-5.54	-17.73	**-29.82**	-13.71	-15.93	-7.15	-7.13	-10.47	-9.33
RCP8.5	2021–2050	-16.50	-11.54	-13.70	-15.34	-10.53	**-27.22**	**-49.63**	-14.06	**-24.84**	-16.28	-8.73	-12.39	-14.67

*α = 0.05; bold parts indicate significant differences in the mean according to the t-test, gray shaded parts indicate non-homogeneous data according to the MW test

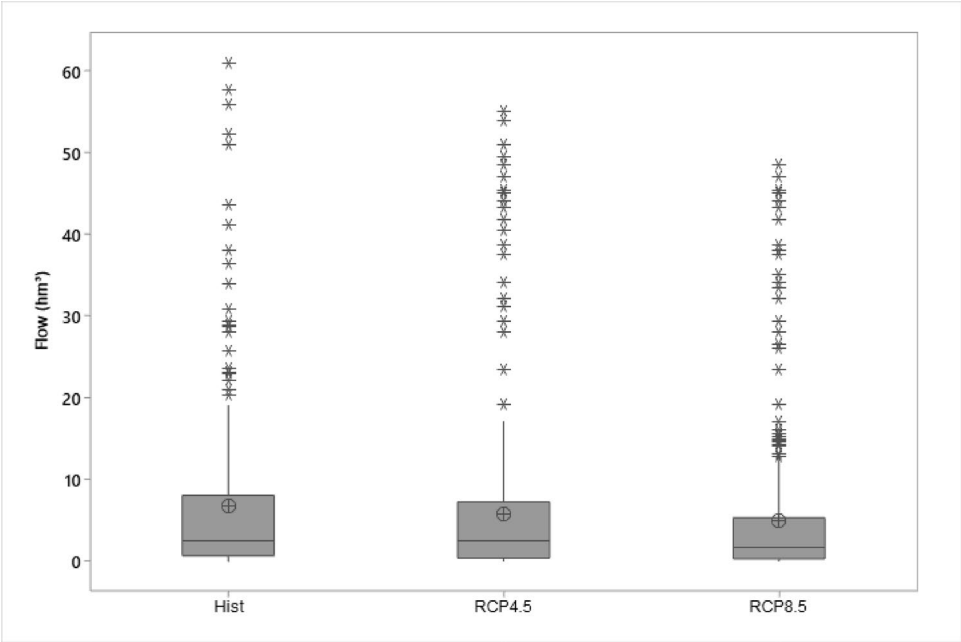

Fig. 3 Box plot representation of scenario-based streamflows in the Sarıgöl Afşar Dam Basin (Circle-enclosed plus signs represent mean values, and stars indicate outliers)

and 59% for the Ganjal River Basin under RCP4.5 and RCP8.5, respectively.

Collectively, these results corroborate the findings of the present study, suggesting that streamflow feeding the Sarıgöl Afşar Dam is likely to decrease under future climate change scenarios, thereby implying potential constraints on irrigation water availability in the basin.

Net irrigation water requirement analysis

The analysis of net IWR initially focused on grapevines, which dominate agricultural production in the study area, while also evaluating potential alternative crops. In this assessment, economic value, drought resistance, and lower ET_c relative to grapes were considered as key criteria. Crops including winter wheat, watermelon, winter barley, potato, melon, eggplant, sunflower, processing tomato, bean, and cabbage were analyzed. Olives were also included due to their extensive cultivation across the Aegean Region, higher drought tolerance than grapes, and greater profitability despite higher water requirements (MAF 2014, 2015, 2023; Tozlukoglu 2022; FAO 2024; TurkStat 2024). Accordingly, olives were identified as the primary substitute crop. Among the alternatives, sunflower exhibited substantially lower ET_c, IWR, and net IWR compared to grapes, primarily owing to its shorter growing season and reduced overall water demand. Consequently, a secondary scenario consisting of winter wheat and sunflower cultivation was emphasized as a feasible alternative, given their higher drought tolerance, lower water requirements, and favorable economic performance (Table 18).

ET_c values for winter wheat, sunflower (as a secondary crop), table/dried grapes, and olives were determined for the observation period. For comparative purposes, ET_c and IWR values calculated for the 1986–2005 period were used as the baseline. Under the RCP4.5 and RCP8.5 scenarios, annual total ET_c values for 2021–2050 were projected assuming unchanged crop patterns. The projections indicated increases for all crops: olives by 1.24% (RCP4.5) and 2.67% (RCP8.5); grapes by 3.97% and 6.43%; winter wheat by 2.90% and 5.00%; and sunflower by 5.98% and 9.41%, respectively (Fig. 4). Among the crops considered, sunflower displayed the lowest drought resistance, whereas olives were more drought-tolerant than grapes.

IWR for winter wheat, table/dried grapes, olives, and sunflower (as a secondary crop) were also evaluated. Grapes were analyzed first for the future scenarios under RCP4.5 and RCP8.5, followed by alternative crop combinations. IWR values for grapes increased by 5.61% under RCP4.5 and 10.12% under RCP8.5. In the olive cultivation scenario, IWR increased by 3.11% (RCP4.5) and 5.40% (RCP8.5). For the wheat–sunflower scenario, IWR increased by 11.61% (RCP4.5) and 13.97% (RCP8.5) for sunflower, and by 4.16% and 7.43% for winter wheat (Fig. 5).

Net IWR values were subsequently calculated for grapes and alternative crops. The irrigation water supplied from the Sarıgöl Afşar Dam was compared between the observation and projection periods under both RCP scenarios. The results showed that the net IWR of grapes increased by 18.21% under RCP4.5 and 25.93% under RCP8.5. For olives, the increases were 7.41% and 9.86%, respectively. Winter wheat and sunflower exhibited increases of 16.49% and 13.21% under RCP4.5, and 23.72% and 15.13% under

Table 18 ET_c values, drought resistance levels, and market prices of agricultural products

Agri. Products	ET_c (mm)	DRS	Export Revenue per ton (*1000 USD)						Domestic Market Value (kg*1 000 000 TL)					
			2018	2019	2020	2021	2022	Average	2018	2019	2020	2021	2022	Average
Olive and Olive Oil	688.70	R	3.61	2.67	2.41	3.08	3.61	3.07	8.95	9.38	8.76	15.26	47.62	17.99
Sunflower	291.75	R	1.01	0.91	0.98	1.48	1.75	1.22	8.94	11.21	17.8	24.92	47.02	21.97
Tomato Paste	578.87	F	1.09	1.23	1.10	0.98	1.50	1.18	4.84	5.41	6.64	9.18	32.48	11.71
Beans	390.57	F	0.76	0.88	0.85	0.79	0.85	0.83	2.79	3.83	4.46	4.54	9.39	5.00
Grape	624.98	F	0.67	0.73	0.74	0.77	0.79	0.74	7.49	9.49	11.31	12.06	30.72	14.21
Melon	511.24	R	0.75	0.72	0.72	0.66	0.73	0.72	1.84	2.08	2.72	2.91	6.41	3.19
Eggplant	591.65	R	0.61	0.67	0.62	0.60	0.71	0.64	1.42	1.60	1.75	2.05	4.60	2.29
Cabbage	198.65	F	0.42	0.37	0.43	0.56	0.47	0.45	3.13	4.19	4.32	5.07	11.95	5.73
Wheat	401.38	R	0.34	0.36	0.32	0.37	0.43	0.36	19.29	23.12	30.83	36.11	106.73	43.22
Watermelon	374.12	F	0.29	0.20	0.28	0.244	0.28	0.26	2.65	2.69	3.52	3.86	9.08	4.36
Barley	387.27	R	0.19	0.25	0.18	0.256	0.35	0.25	6.01	8.14	10.61	10.83	41.41	15.40
Potatoes	506.14	F	0.10	0.23	0.19	0.178	0.13	0.17	1.40	2.61	1.73	1.89	6.64	2.86

Agri. Products = Agricultural Products, DRS = Drought Resistance Status, R = Resistant, F = Flimsy

RCP8.5 (Fig. 6). These findings clearly demonstrate that grapes experience the steepest rise in net IWR compared with the alternative crops considered. The winter wheat–sunflower combination was therefore considered as a comparative reference scenario illustrating the lower water-demand characteristics of annual crops at the crop level, rather than as a system-wide optimal adaptation option, given regional agronomic and socio-economic constraints.

Monthly variations in net IWR were also examined. Average monthly net IWR increased across all months, with September showing the most significant rise, particularly for grapes. For olives, all months except March, April, November, and December exhibited increases, with July recording the highest values. For winter wheat in the wheat–sunflower scenario, net IWR increased in all months except December–February, with the largest rise observed in March. Sunflowers also showed increases in all months relative to the baseline period, with September again showing the largest increase. Overall, olives were identified as the most drought-tolerant crop based on monthly comparisons (Fig. 7).

Based on these results, an alternative cropping pattern was proposed in which olives would occupy 60% of the total irrigated area (11,830 ha) and grapes the remaining 40%. This crop ratio was defined as a representative and feasible adaptation scenario reflecting existing perennial crop dominance and current farming practices in the basin, rather than as an optimized solution. The crop ratio proposed in this study was determined by considering the efficient use of water resources, current agricultural practices in the region, and economic return analyses. Under this configuration, the total net IWR increased by 11.9% under RCP4.5 and 15.6% under RCP8.5 compared to the observation period (Fig. 8).

Previous research supports these findings by highlighting the superior drought tolerance of several Southeastern Anatolian olive varieties (e.g., Halhalı, Eğriburun, Kilis Yağlık, Sarı Habeşi, and Kan Çelebi). In addition, olive cultivars from Tunisia, Algeria, and Morocco, adapted to hot and arid conditions, have been identified as suitable alternatives (Kurucu et al. 2019). The drought resistance of olive trees has also been confirmed by other studies (Parlak 2014; Pouyafard et al. 2016). As a secondary strategy, cultivating sunflower in summer and wheat in winter is recommended. Breeding studies have demonstrated the high drought resistance of specific wheat cultivars (e.g., Taner and Bozkır), which can be further enhanced through cultural practices (Yazar et al. 2013; Kizil 2022). Similarly, research on sunflower has identified promising drought-tolerant cultivars such as Sanbro MR (Ergin and Kaya 2020).

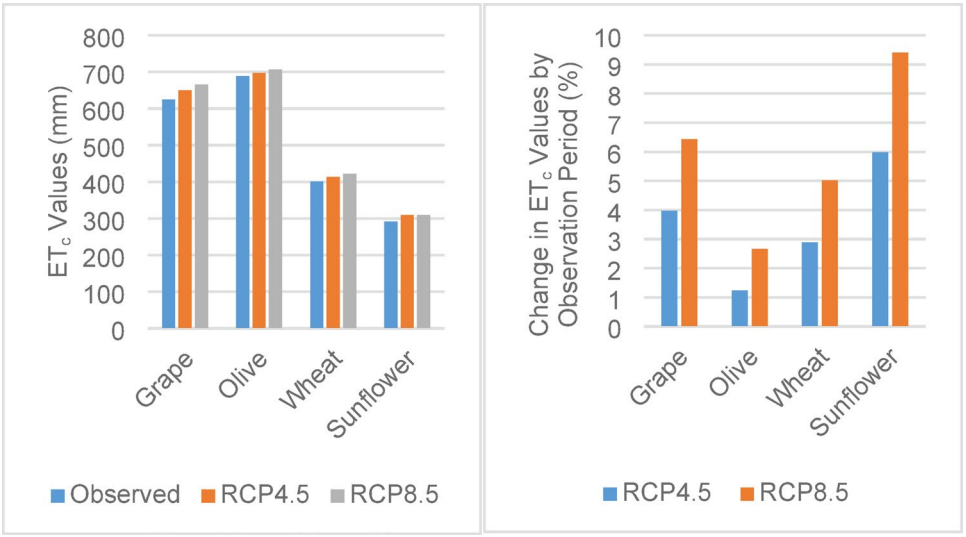

Fig. 4 ET_c values (mm) and their temporal variation during the observation period

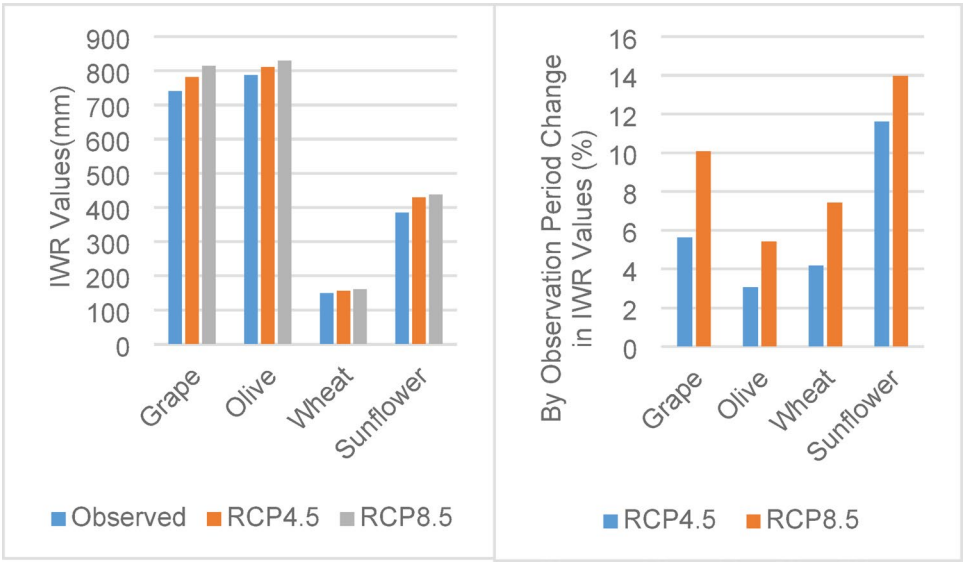

Fig. 5 Temporal variation in IWR (mm) compared to the observation period

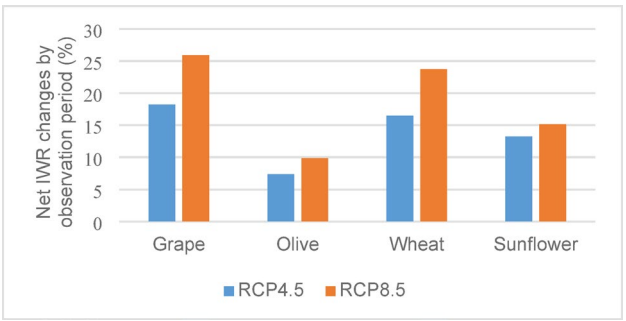

Fig. 6 Temporal variation in net IWR values (%) relative to the observation period

Conclusion

Across the globe, including Türkiye, the impacts of climate change are becoming increasingly severe and are expected to intensify in the coming decades. Developing effective mitigation and adaptation strategies requires accurate assessments of both the extent and magnitude of these impacts. Within this context, the present study generated future projections of hydro-meteorological parameters for the Sarıgöl Afşar Dam Basin—an irrigation-dominated system—and compared them with historical observations. These projections were subsequently used to estimate IWR under various cropping pattern scenarios and to evaluate differences between baseline and future climate conditions.

The findings demonstrate that net IWR values are projected to increase relative to the baseline across all cropping pattern alternatives. However, these alternatives

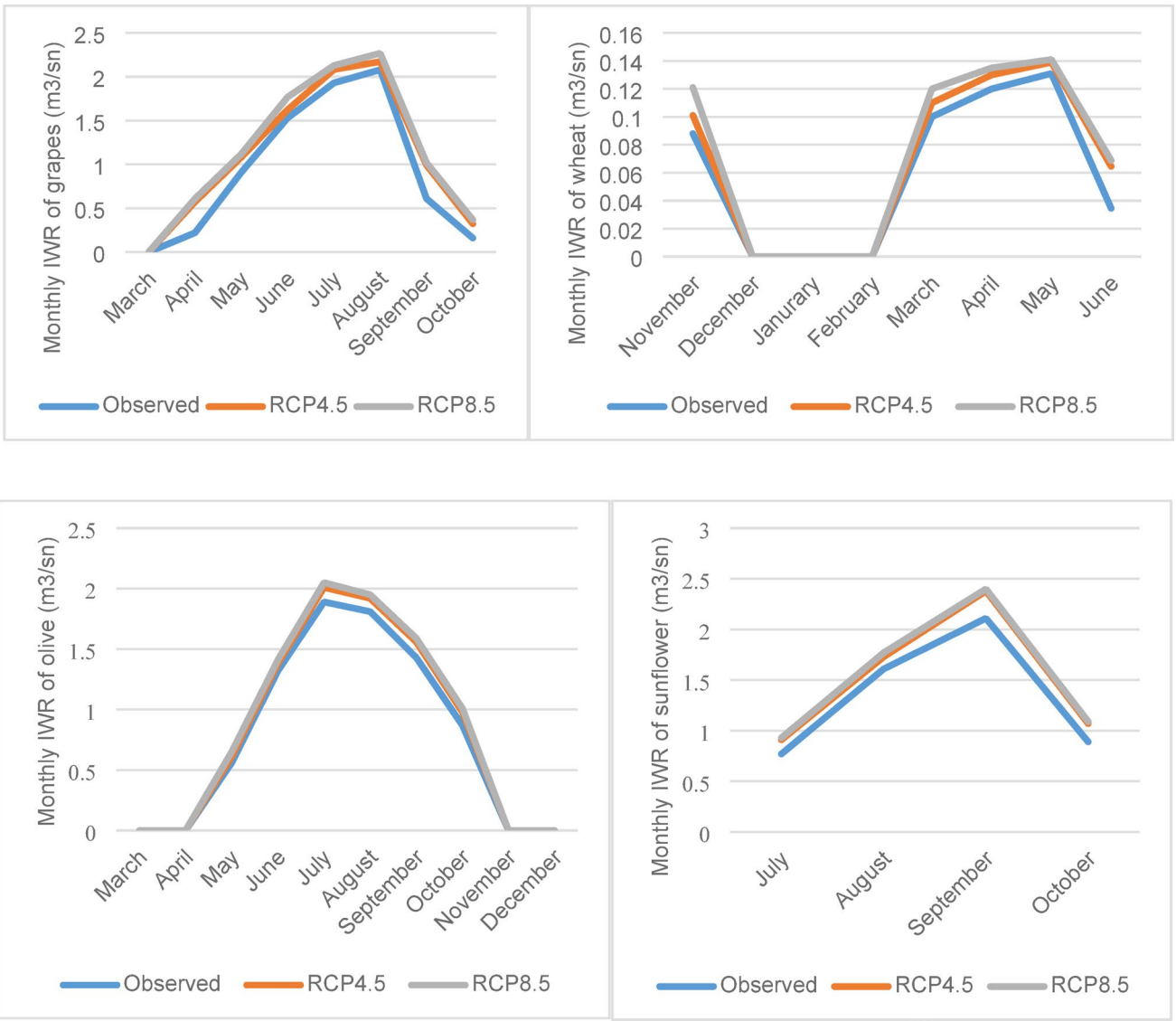

Fig. 7 Monthly total values of net IWR values

consistently exhibited lower net IWR than the continuation of grape monoculture, emphasizing the necessity of modifying or diversifying current cropping systems to achieve sustainable agricultural production and more efficient water management in the region.

Scenario-based streamflow projections also revealed potential reductions in reservoir inflow and storage volumes at the Sarıgöl Afşar Dam. Such declines underscore the basin's decreasing capacity to meet irrigation demands under future climate conditions. Therefore, understanding the implications of these changes for crop water use and net IWR is crucial both for maintaining current agricultural practices and for planning the transition toward more drought-tolerant alternatives.

Among the scenarios assessed, the most favorable option for the study area involves a mixed cropping system—maintaining grape cultivation over 40% of the irrigated area while converting 60% to olive cultivation. The 60% olive–40% grape ratio was not defined as an optimized solution but rather as a representative and feasible adaptation scenario. This proportion reflects the dominance of perennial crops in the basin and farmers' existing production practices, while allowing a partial reduction in irrigation water demand without assuming abrupt or unrealistic changes in land use. This recommendation is consistent with prevailing agricultural practices and supported by comparative economic returns. Relative to the baseline, this configuration is projected to increase net IWR by 11.28% under RCP4.5 and 15.59% under RCP8.5, while continued grape cultivation alone would increase net IWR by 18.21% and 25.93%, respectively.

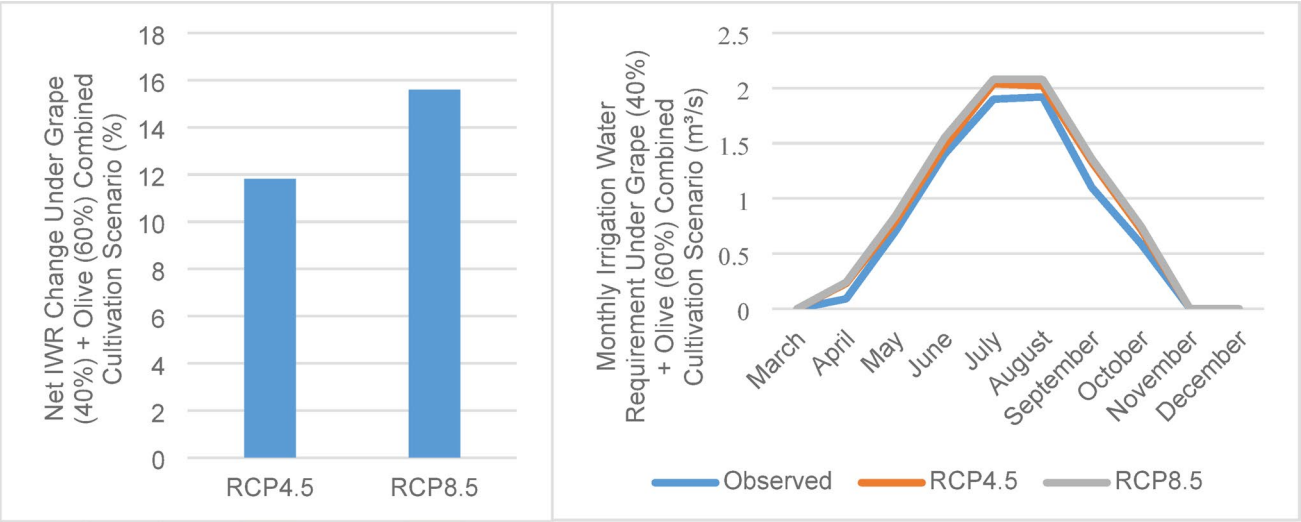

Fig. 8 Percentage change and monthly variation in net IWR under the combined cultivation scenario of grape (40%) and olive (60%)

Accordingly, the mixed perennial cropping system was identified as the most feasible and regionally applicable adaptation pathway at the system scale, while scenarios involving winter wheat and sunflower primarily serve as a comparative reference reflecting the lower water-demand characteristics of annual crops at the crop level.

Overall, these results highlight the potential of adaptive cropping strategies to mitigate the adverse effects of climate change while recognizing that such impacts are inevitable for the basin. Furthermore, the methodological framework employed in this study provides a practical and transferable approach for researchers working in other climate-sensitive regions and offers valuable insights for farmers and policy-makers seeking to design sustainable adaptation strategies.

Supplementary Information The online version contains supplementary material available at https://doi.org/10.1007/s40899-026-01324-w.

Funding No funding was received for conducting this study.

Data availability The data supporting the findings of this study are available from the corresponding author upon reasonable request for scientific purposes, provided that a valid justification is given.

Declarations

Conflict of interest The authors have no competing interests to declare that are relevant to the content of this article.

References

Abdulla FA, Lettenmaier DP (1997) Development of regional parameter estimation equations for a macroscale hydrologic model. J Hydrol 197:230–257. https://doi.org/10.1016/S0022-1694(96)03262-3

Abeysingha NS, Islam A, Singh M (2020) Assessment of climate change impact on flow regimes over the Gomti River basin under IPCC AR5 climate change scenarios. J Water Clim Chang 11:303–326. https://doi.org/10.2166/wcc.2018.039

Ahn KH, Merwade V (2014) Quantifying the relative impact of climate and human activities on streamflow. J Hydrol 515:257–266. https://doi.org/10.1016/j.jhydrol.2014.04.062

Allen RG, Pereira LS, Raes D, Smith M (1998) Crop evapotranspiration: guidelines for computing crop water requirements (FAO Irrigation and Drainage Paper No. 56)

Ayva C, Dutucu A, Ustaoglu B (2023) Climate change impact on water resources and adaptation strategies : the case of Kirazdere. J Soc Sci 1:47–65

Bayram A (2022) Water resources are shrinking in Manisa, which spent the fall without rainfall. In: Anadolu agency. https://www.aa.com.tr/tr/gundem/sonbahari-yagissiz-geciren-manisada-su-kaynaklari-cekiliyor/2741061

Blaney HF and Criddle WD (1950) Determining water requirements in irrigated areas from climatological and irrigation data. Washington D.C.: U.S. Soil Conservation Service

Bozoglu M, Baser U, Alhas Eroglu N, Kilic Topuz B (2019) Impacts of climate change on Turkish agriculture

Burnham KP, Anderson DR (2002) Model selection and multimodel inference: a practical information-theoretic approach. Springer, New York

Caprio JM (1974) The solar thermel unit concept in problems related to plant development and potential evapotranspiration. In: Phenology and seasonality modeling

Chou SC, Lyra A, Mourão C et al (2014) Assessment of climate change over South America under rcp 4.5 and 8.5 downscaling scenarios. Am J Clim Change 03:512–527. https://doi.org/10.4236/ajcc.2014.35043

Demirgul T, Berkay Yilmaz C, Zipir BN et al (2022) Investigation of Türkiye's climate periods in terms of precipitation and temperature changes. Eng Appl 1:80–90

Doulabian S, Golian S, Toosi AS, Murphy C (2021) Evaluating the effects of climate change on precipitation and temperature for Iran using rcp scenarios. J Water Clim Chang 12:166–184. https://doi.org/10.2166/wcc.2020.114

Ergin N, Kaya MD (2020) Effects of drought and temperature stresses on germination and seedling development of sunflower. Turk J Agric Food Sci Technol 8:598–602. https://doi.org/10.24925/turjaf.v8i3.598-602.3031

FAO (2025) Landcover/use, land cover (Global–10m–2021)—ESA world cover. https://data.apps.fao.org/?lang=en
FAO56 (1998) FAO irrigation and drainage paper crop by. Irrig Drain 300:300
FAO F and AO (2024) FAOSTAT, trade, crops and livestock products. In: Food and Agriculture Organization. https://www.fao.org/faostat/en/#data/TCL
Fenicia F, Kavetski D, Savenije HG (2011) Elements of a flexible approach for conceptual hydrological modeling: 1. motivation and theoretical development. Water Resour Res 47:W11510. https://doi.org/10.1029/2010WR010174
Fide EB (2022) Turkish press climate change coverage (2018–2019): elements of disconnect in discourses and the representation of solutions. New Perspect Turk 67:32–56. https://doi.org/10.1017/npt.2022.8
Fisher RA (1925) Statistical methods for research workers. Oliver & Boyd, Edinburgh
GDARP GD of AR and P, SHW SHW (2016) A guide to plant water consumption of irrigated crops in Türkiye. Ankara
Hamon WR (1961) Estimating potential evapotranspiration. J Hydraul Div 87:107–120
Hargreaves GH, Samani ZA (1985) Reference crop evapotranspiration from temperature. Appl Eng Agric 1:96–99
Helsel DR and Hirsch RM (2002) Statistical methods in water resources. USGS techniques of water-resources investigations Book 4, Chapter A3
Heydari MM, Aghamajidi R, Beygipoor G, Heydari M (2014) Comparison and evaluation of 38 equations for estimating reference evapotranspiration in an Arid Region. Fresenius Environ Bull 23:1985–1996
Hocking RR (1976) The analysis and selection of variables in linear regression. Biometrics 32:1–49. https://doi.org/10.2307/2529336
Irmak S, Irmak A, Allen RG, Jones W (2003) Solar and net radiation-based equations to estimate reference evapotranspiration in humid climates. J Irrig Drain Eng 129:336–347
Islam A, Turan A, Sonkaya M, Dizdar A (2021) Evaluation of global climate change in terms of hazelnut agriculture: Altınordu case. Global climate change and its effects on Dokap Region. Dokap Region Universities Union, Giresun, pp 66–81
Jensen ME, Haise HR (1963) Estimating evapotrannspiration from solar radiation. J Irrig Drain Div 89:15–41
Jiang M, Felzer BS, Sahagian D (2016) Predictability of precipitation over the conterminous U.S. based on the CMIP5 multi-model ensemble. Sci Rep 6:1–9. https://doi.org/10.1038/srep29962
Kendall MG (1975) Rank correlation methods. Griffin, London
Kirdemir U (2017) Modeling the possile impacts of climate change on dam basin hydrology: AR5-RCP scenarios and the case of Demirköprü Dam. Balikesir University
Kiymaz H (2018) Investigation of potential evapotranspiration equations suitable for conceptual hydrological models. Balikesir University
Kizil A (2022) Investigation of the effects of nitrogen fertilizer applications on drought stress in some wheat cultivars. Artvin Coruh University
Knutti R, Furrer R, Tebaldi C et al (2010) Challenges in combining projections from multiple climate models. J Clim 23:2739–2758. https://doi.org/10.1175/2009JCLI3361.1
Kurucu Y, Delibacak S, Asik S, Akkuzu E, Duman I, Hepaksoy S et al (2019) Drought management proposal for uninterrupted agricultural production compatible with changing climatic conditions: the case of small meander Basin. Project No. 16-ZRF-043, Final Project Report. Ege University, Scientific Research Projects Coordination Unit, Izmir, Türkiye
Kuskova NE, Toropov PA, Oleinikov AD (2021) Meteorological conditions of extreme avalanche formation in Caucasian mountains (according to observation and reanalysis data). Water Resources 49(Suppl 1):S99–S111. https://doi.org/10.1134/S0097808222070089
Lee H, Calvin K, Dasgupta D et al (2022) IPCC Sixth assessment report—synthesis report
Liu G, Powell B, Friedrich T (2023) Climate downscaling for regional models with a neural network: a Hawaiian example. Prog Oceanogr 215:103047. https://doi.org/10.1016/j.pocean.2023.103047
MAF M of A and F (2014) Control of potato diseases and pests. In: Minist. Agric. For. https://kilis.tarimorman.gov.tr/Sayfalar/PageNotFoundError.aspx?requestUrl=https://kilis.tarimorman.gov.tr/Belgeler/Yetiştiricilik Dökümanları/patates.pdf
MAF M of A and F (2015) Bean cultivation. In: MAF or Ministry of Agriculture and Fisheries/Forestry. https://isparta.tarimorman.gov.tr/Belgeler/Faydalı Bilgiler/Bitkisel Yetiştiricilik/Tarla Bitkileri Yetiştiriciliği/Fasulye Yetiştiriciliği.pdf
MAF M of A and F (2023) Manisa sultani seedles grape. https://manisa.tarimorman.gov.tr/Menu/32/Manisa-Sultani-Cekirdeksiz-Uzumu?utm_source=chatgpt.com
Makkink GF (1957) Testing the penman formula by means of lysimeters. J Inst Water Eng 11:277–288
Mann HB (1945) Nonparametric tests against trend. Econometrica 13:245–259
Maraun D, Wetterhall F, Ireson AM, Chandler RE, Kendon EJ, Widmann M, Brienen S, Rust HW, Sauter T, Themeßl M, Venema V, Chun KP, Goodess CM, Jones RG, Onof C, Vrac M, Thiele-Eich I (2010) Precipitation downscaling under climate change: recent developments to bridge the gap between dynamical models and the end user. Rev Geophys 48:RG3003. https://doi.org/10.1029/2009RG000314
McGuinness JL and Bordne EF (1972) A comparison of lysimeter derived potential evapotranspiration with computed values. Technical Bulletin 1452. Agricultural Research Service. US Department of Agriculture. Washington, DC
McMahon TA, Peel MC, Lowe L et al (2013) Estimating actual, potential, reference crop and pan evaporation using standard meteorological data: a pragmatic synthesis. Hydrol Earth Syst Sci 17:1331–1363. https://doi.org/10.5194/hess-17-1331-2013
Monteith JL (1965) Evaporation and the environment, in the state and movement of water in living organism. In: Proceedings of the 19th symposium, society of experimental biology. Society for experimental biology. Cambridge University Press
Moriasi DN, Arnold JG, Van Liew MW, Bingner RL, Harmel RD. VTL (2007) Model evaluation guidelines for systematic quantification of accuracy in watershed simulations. Trans ASABE 50:885–900. https://doi.org/10.13031/2013.23153
Nacar S, Kankal M, Okkan U (2022) Evaluation of the suitability of NCEP/NCAR, ERA-Interim and ERA5 reanalysis data sets for statistical downscaling in the Eastern Black Sea Basin, Türkiye. Meteorol Atmos Phys 134:1–23. https://doi.org/10.1007/s00703-022-00878-6
Noto LV, Cipolla G, Pumo D, Francipane A (2023) Climate change in the Mediterranean Basin (Part II): a review of challenges and uncertainties in climate change modeling and impact analyses. Water Resour Manag 37:2307–2323. https://doi.org/10.1007/s11269-023-03444-w
Okkan U (2013) Evaluation of the effects of climate change on river flows. Dokuz Eylul University
Okkan U (2015) Dynamic water budget model. BAU Inst Sci J 17:70–82
Okkan U, Inan G (2015) Statistical downscaling of monthly reservoir inflows for Kemer watershed in Türkiye: use of machine learning methods, multiple GCMs and emission scenarios. Int J Climatol 35:3274–3295. https://doi.org/10.1002/joc.4206
Okkan U, Kiymaz H (2020) Questioning of empirically derived and locally calibrated potential evapotranspiration equations for a lumped water balance model. Water Supply 20:1141–1156

Okkan U, Tatli H, Dalkilic HY (2016) Examining future irrigation and drinking water sufficiency under climate change scenarios: the Gediz Basin example. TUBITAK Project No: 114Y716 Final Report

Oudin L, Hervieu F, Michel C et al (2005a) Which potential evapotranspiration input for a lumped rainfall-runoff model? Part 2—towards a simple and efficient potential evapotranspiration model for rainfall-runoff modelling. J Hydrol 303:290–306. https://doi.org/10.1016/j.jhydrol.2004.08.026

Oudin L, Michel C, Anctil F (2005b) Which potential evapotranspiration input for a lumped rainfall-runoff model? Part 1—can rainfall-runoff models effectively handle detailed potential evapotranspiration inputs? J Hydrol 303:275–289. https://doi.org/10.1016/j.jhydrol.2004.08.025

Ozdemir A (2021) Evaluation of climate change impacts on runoff and sediment at the basin scale: Yuvacık dam lake basin. J Geol Eng 45:129–153. https://doi.org/10.24232/jmd.941528

Panagos P, Borrelli P, Matthews F et al (2022) Global rainfall erosivity projections for 2050 and 2070. J Hydrol 610:127865. https://doi.org/10.1016/j.jhydrol.2022.127865

Pandey PK, Dabral PP, Pandey V (2016) Evaluation of reference evapotranspiration methods for the northeastern region of India. Int Soil Water Conserv Res 4:52–63. https://doi.org/10.1016/j.iswcr.2016.02.003

Parlak M (2014) Change in plant water stress index (CWSI) due to water stress in Ayvalık olive seedlings and determination of the relationship between CWSI and stomatal conductance. Ege University

Penman HL (1948) Natural evaporation from open water, bare soil and grass, proccedings of the royal society a: mathematical. Phys Eng Sci 193:120–145

Perrin C, Michel C, Andreassian V (2001) Does a large number of parameters enhance model performance? Comparative assessment of common catchment model structures on 429 catchments. J Hydrol 242:275–301. https://doi.org/10.1016/S0022-1694(00)00393-0

Pouyafard N, Akkuzu E, Kaya U (2016) Identification of some physiological and morphological changes due to water stress in Ayvalık olive seedlings grown under Aegean coastal conditions. J Tekirdag Fac Agric 13:88–98

Priestley CHB, Taylor RJ (1972) On the assessment of surface heat flux and evaporation using large-scale parameters. Mon Weather Rev 100:81–92

Raziei T, Parehkar A (2021) Performance evaluation of NCEP/NCAR reanalysis blended with observation-based datasets for estimating reference evapotranspiration across Iran. Theor Appl Climatol 144:885–903. https://doi.org/10.1007/s00704-021-03578-0

Romanic D, Hangan H, Ćurić M (2018) Wind climatology of Toronto based on the NCEP/NCAR reanalysis 1 data and its potential relation to solar activity. Theor Appl Climatol 131:827–843. https://doi.org/10.1007/s00704-016-2011-7

Serbes AZ, Okkan U, Asik S (2018) Estimation of net irrigation water demand under possible climate change scenarios: case of Menemen Left Bank. J Süleyman Demirel Univ Fac Agric Spec Issue 1st Int Agric Struct Irrig Congr 91–101

SHW (2021) Sarıgöl Afşar Dam details. State Hydraulic Works. Türkiye. https://www.dsi.gov.tr/baraj/detay.cfm?BarajID=58 (accessed 9 January 2021)

Singh A, Singh G (2022) Climate change impact assessment on streamflow of Ganjal River, India. Ecol Environ Conserv 28:707–718. https://doi.org/10.53550/eec.2022.v28i02.020

Student (1908) The probable error of a mean. Biometrika 6:1–25

Thornthwaite CW (1948) An approach toward a rational classificaiton of climate. Soil Sci 66–77

Tokar AS, Momcilo M (2000) Precipitation-runoff modeling using artificial neural networks and conceptual models. J Hydrol Eng 156–161

Tozlukoglu S (2022) Tozlukoglu. In: Tavas Chamb. Agric. http://tavas.ziraatodasi.org.tr/zeytin#:~:text=Kurakl ığa dayanıklıdır.,ve uzun süre depolamaya uygundur

Turc L (1961) Water requirements assessment of irrigation, potential evapotranspiration: simplified and updated climatic formula. Ann Agron 12:13–49

TurkStat TSI (2024) Crop production prices and production value. In: Turkish Stat. Inst. https://data.tuik.gov.tr/Bulten/Index?p=Bitkisel-Urun-Fiyatlari-ve-Uretim-Degeri-2021-45506

Wald A, Wolfowitz J (1940) On a test whether two samples are from the same population. Ann Math Stat 11:147–162

Wang Y, Liu L, Guo P et al (2019) An inexact irrigation water allocation optimization model under future climate change. Stoch Environ Res Risk Assess 33:271–285. https://doi.org/10.1007/s00477-018-1597-y

Wilcoxon F (1945) Individual comparisons by ranking methods. Biometrics 1:80–83

Xu C, Singh VP (2000) Evaluation and generalization of radiation-based methods for calculating evaporation. Hydrol Process 14:339–434

Xu C, Singh VP (2001) Evaluation and generalization of temperaturebased methods for calculating evaporation. Hydrol Process 15:305–319

Xu C, Singh VP (2002) Cross comparison of empiricial equations for calculating potential evapotranspiration with data from Switserland. Water Resour Manag 16:197–219

Xystrakis F, Matzarakis A (2011) Evaluation of 13 empirical reference potential evapotranspiration equations on the Island of Crete in Southern Greece. J Irrig Drain Eng 137:211–222

Yazar S, Salantur A, Ozdemir B et al (2013) Investigation of some agricultural characteristics in bread wheat breeding studies in Central Anatolia Region. J F Crop Cent Res Inst 22:32–40

You Q, Min J, Fraedrich K et al (2014) Projected trends in mean, maximum, and minimum surface temperature in China from simulations. Glob Planet Change 112:53–63. https://doi.org/10.1016/j.gloplacha.2013.11.006

Zainal E, Toshiharu K (2017) Investigation of long-term evapotranspiration by using Hamon equation factor and NDVI data in forest plantations area. China-USA Bus Rev 10:409–506. https://doi.org/10.17265/1537-1514/2016.10.002

Zhai X, Li Y, Wang H et al (2023) Assessment of the potential impacts of climate changes on Syr Darya watershed: a hybrid ensemble analysis method. J Hydrol Reg Stud. https://doi.org/10.1016/j.ejrh.2023.101415